Experimental Investigation of Donor–Acceptor Electron Transfer and Back Transfer in Solid Solutions

R. C. Dorfman, Y. Lin, and M. D. Fayer*

Department of Chemistry, Stanford University, Stanford, California 94305 *(Received: January 17, 1989)*

Electron transfer from an optically excited donor (rubrene) to randomly distributed acceptors (duroquinone) followed by electron back transfer in a rigid solution (sucrose octaacetate) has been studied experimentally. The forward electron-transfer process was observed by time-dependent fluorescence quenching measurements, while the electron back transfer from the radical anion to the radical cation was monitored by use of the picosecond transient grating technique. A statistical mechanics theory is used to describe the time-dependent dynamics of the system and to extract the forward- and back-transfer parameters from the data. The theory includes donor–acceptor and acceptor–acceptor excluded volume. It is found that the inclusion of excluded volume is necessary to obtain accurate transfer parameters. These parameters enable a detailed description of the electron transfer and recombination dynamics to be given. The agreement between theory and experiment is excellent. A variety of time-dependent properties of the system are calculated. These include the time-dependent ion populations and the probability that the ith acceptor is an ion as a function of time and distance. In addition, $\langle R(t)\rangle$ and $\langle \tau(t)\rangle$, which are the average ion separation as a function of time and the average ion existence time as a function of ion separation, respectively, are calculated.

I. Introduction

In this paper we will focus on a system in which there are donors (low concentration) and acceptors (high concentration) randomly distributed in a solid solution. Optical excitation of a donor can be followed by transfer of an electron to an acceptor.[1] Once electron transfer has occurred, there exists a ground-state radical cation (D^+) near a ground-state radical anion (A^-). Since the thermodynamically stable state is the neutral ground-state D and A, back transfer will occur. In liquid solution, back transfer competes with separation by diffusion. Separated ions are extremely reactive and can go on to do useful chemistry.[2]

Over the past 30 years a considerable amount of research has been performed in the area of electron transfer. In particular, a great deal of work, both theoretical[3-9] and experimental[10-17] has been directed toward elucidating the microscopic electron-transfer rate. The dependence of exothermicity,[7,8,19] temperature,[9-11] distance,[6,12,16,20-22] angles,[12] and solvent relaxation[4,5,13-15] on the rate have been explored in a variety of systems.

A number of treatments have considered donors and acceptors held fixed by rigid molecular bridges (intramolecular transfer).[6,8,13,19,23-25] In these cases the effect of molecular spacer,[6] electric field,[23,26] or solvent relaxation[13,24] was measured independent of distance effects. There have also been studies on nonlinked donors and acceptors (intermolecular transfer). Pulse radiolysis has been used to create trapped electrons in glasses.[27] The acceptors and solvent molecules have been varied to study the effect of reaction exothermicity on the electron-transfer rate from the trap to the acceptor. Studies have also investigated the recombination rate of photoproduced geminate cation–electron pairs.[28,29] Photoinduced electron transfer has been studied in solution between colloidal semiconductors and dye molecules.[30] "Solvent-free"[11] systems have also been studied to isolate the effects of the solvent.

While a great deal is known about electron transfer, there has been considerable interest in the process of electron transfer followed by back transfer (which is not well understood). A number of investigations of photosynthetic electron-transfer pathways, both time resolved and steady state, have been reported.[1,10,26,31] In photosynthesis, the complex structure of the system of a donor and a sequence of acceptors inhibits back transfer, and efficient charge separation takes place. There have also been studies of transfer and recombination in liquid solutions between geminate ion pairs[29] and geminate cation–electron pairs.[28,30,32-35] Because of the complexity of the problem of coupled forward and back transfer in a system undergoing molecular diffusion, a detailed statistical mechanical theory describing the dynamics is lacking. Here the focus is on a system of donors and acceptors that are in fixed positions. This permits the ensemble-averaged dynamics of the coupled forward- and back-

(1) Guarr, T.; McLendon, G. *Coord. Chem. Rev.* **1985**, *68*, 1.
(2) Devault, D. *Q. Rev. Biophys.* **1980**, *13*, 387.
(3) Kestner, N. R.; Logan, J.; Jortner, J. *J. Phys. Chem.* **1974**, *78*, 2148.
(4) Yan, Y. J.; Sparpaglione, M.; Mukamel, S. *J. Phys. Chem.* **1988**, *92*, 4842.
(5) Sparpaglione, M.; Mukamel, S. *J. Chem. Phys.* **1988**, *88*, 3263.
(6) Beratan, D. N. *J. Am. Chem. Soc.* **1986**, *108*, 4321.
(7) Siders, P.; Marcus, R. A. *J. Am. Chem. Soc.* **1981**, *103*, 748.
(8) McConnell, H. *J. Chem. Phys.* **1961**, *35*, 508.
(9) Brunschwig, B. S.; Ehrenson, S.; Sutin, N. *J. Am. Chem. Soc.* **1984**, *106*, 6858.
(10) Fleming, G. R.; Martin, J. L.; Breton, J. *Nature* **1988**, *333*, 190.
(11) Kemmitz, K.; Nakashima, N.; Yoshihara, K. *J. Phys. Chem.* **1988**, *92*, 3915.
(12) Domingue, R. P.; Fayer, M. D. *J. Chem. Phys.* **1985**, *83*, 2242.
(13) Simon, J. D.; Su, S. *J. Chem. Phys.* **1987**, *87*, 7016.
(14) McGuire, M.; McLendon, G. *J. Phys. Chem.* **1986**, *90*, 2549.
(15) Huppert, D.; Ittah, V.; Masad, A.; Kosower, E. M. *Chem. Phys. Lett.* **1988**, *150*, 349.
(16) Huddleston, R. K.; Miller, J. R. *J. Phys. Chem.* **1982**, *86*, 200.
(17) Kemnitz, K. *Chem. Phys. Lett.* **1988**, *152*, 305.
(18) Mataga, N.; Kanda, Y.; Okada, T. *J. Phys. Chem.* **1986**, *90*, 3880.
(19) Chen, P.; Danielson, E. *J. Phys. Chem.* **1988**, *92*, 3708.
(20) Siders, P.; Cave, R. J.; Marcus, R. A. *J. Chem. Phys.* **1984**, *81*, 5613.
(21) Zamaraev, K. I.; Khairutdinov, R. F.; Miller, J. R. *Chem. Phys. Lett.* **1978**, *57*, 311.
(22) Strauch, S.; McLendon, G.; McGuire, M.; Guarr, T. *J. Phys. Chem.* **1983**, *87*, 3579.
(23) Lockhart, D. J.; Goldstein, R. F.; Boxer, S. G. *J. Chem. Phys.* **1988**, *89*, 1408.
(24) Su, S.; Simon, J. *J. Chem. Phys.* **1988**, *89*, 908.
(25) Hofstra, U.; Schaafsma, T. J.; Sanders, G. M.; Van Dijk, M.; Van Der Plas, H. C.; Johnson, D. G.; Wasielewski, M. R. *Chem. Phys. Lett.* **1988**, *151*, 169.
(26) Popovic, Z. D.; Kovacs, G. J.; Vincett, P. C. *Chem. Phys. Lett.* **1985**, *116*, 405.
(27) Miller, J. R.; Beitz, J. V.; Huddleston, R. K. *J. Am. Chem. Soc.* **1984**, *106*, 5057.
(28) Braun, C. L.; Scott, T. W. *J. Phys. Chem.* **1987**, *91*, 4436.
(29) Hirata, Y.; Mataga, N.; Sakata, Y.; Misumi, S. *J. Phys. Chem.* **1986**, *90*, 6065.
(30) Nosaka, Y.; Miyama, H.; Terauchi, M.; Kobayashi, T. *J. Phys. Chem.* **1988**, *92*, 255.
(31) Fischer, S. F.; Scherer, P. O. J. *Chem. Phys.* **1987**, *115*, 151.
(32) Kakitani, T.; Mataga, N. *J. Phys. Chem.* **1985**, *89*, 8.
(33) Miyasaka, H.; Mataga, N. *Chem. Phys. Lett.* **1987**, *134*, 480.
(34) Schulten, Z.; Schulten, K. *J. Chem. Phys.* **1977**, *66*, 4616.
(35) Werner, H. J.; Schulten, Z.; Schulten, K. *J. Chem. Phys.* **1977**, *67*, 646.

0022-3654/89/2093-6388$01.50/0

transfer processes to be isolated from the influence of molecular diffusion. In a subsequent publication, we will present an extension of this work to include diffusion in liquid solutions.[36]

While the forward-transfer process is relatively straightforward to study using time-resolved fluorescence quenching,[37] the back-transfer process requires the application of a method that is sensitive to the ground-state ion concentrations. It will be demonstrated that a picosecond transient grating (TG) experiment is ideally suited for observation of the back-transfer dynamics. The TG method has also been used to measure related phenomena such as electron–hole pair dynamics in amorphous semiconductors[38] and energy transfer and trapping in dye solutions.[39]

The forward-transfer process involves the interaction of a donor with acceptors that are randomly distributed in space. For a donor–acceptor electron-transfer rate, which falls off exponentially with distance, Inokuti and Hirayama[37] have developed a statistical mechanics theory that describes the time dependence of the ensemble-averaged forward-transfer dynamics.

The back-transfer problem is more complex. The distribution of distances between the ions D^+ and A^- is not random. It is determined by the details of the forward-transfer process. The distribution will be strongly biased toward small separations. After electron transfer the system consists of a cation near an anion. In a previous publication we developed a theory that takes these factors into account.[40] The theory calculates the ensemble-averaged time-dependent probabilities of finding the system in the neutral ground state, the electronic excited state, and the electron-transfer state composed of a cation (D^+) and an anion (A^-).

Using these state probabilities, descriptions of the observables for fluorescence yield measurements, time-resolved fluorescence, and transient grating experiments have been derived and compared to data. Excellent agreement between theory and experiment is obtained. It will be shown that, using the measured parameters and the theoretical expressions for the probabilities, it is possible to calculate a number of interesting time-dependent properties that are characteristic of electron transfer and back transfer in an ensemble of donors and acceptors randomly distributed in a rigid solution. Calculations of the time-dependent ion populations and the probability that the ith acceptor is an anion as a function of time and distance are presented. In addition, $\langle R(t)\rangle$ and $\langle \tau(R)\rangle$ which are the average ion separation as a function of time and the average ion existence time as a function of ion separation, respectively, are calculated. The calculations, displayed in Figures 5–11, provide detailed insights into the electron-transfer–back-transfer dynamics of a real physical system.

II. Theory

A detailed account of the theory has been presented elsewhere.[40] Here, only the important features shall be discussed. In the model, donors and acceptors are randomly distributed and held fixed in a rigid matrix. It is assumed that the donor has only one accessible excited state and the acceptor has only one acceptor state. The transfer rates are exponentially decaying functions of distance.[3,12,16,20,22,41] After pulsed excitation of the donor, three processes occur in the system: excited-state decay, forward electron transfer, and electron back transfer. From these processes, the following rate constants are defined (see Figure 1):

$$k = \frac{1}{\tau} \qquad \text{excited-state decay} \tag{1a}$$

$$K_f = \frac{1}{\tau}\exp\left(\frac{R_0 - R}{a_f}\right) \qquad \text{forward transfer} \tag{1b}$$

$$K_b = \frac{1}{\tau}\exp\left(\frac{R_b - R}{a_b}\right) \qquad \text{back transfer} \tag{1c}$$

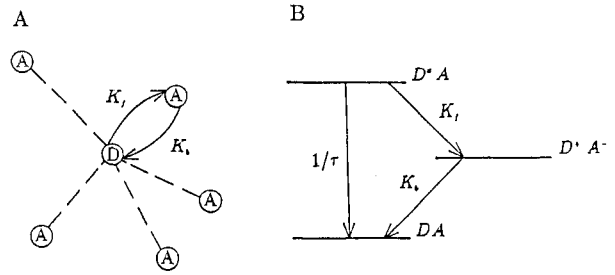

Figure 1. (A) Schematic representation of electron transfer with recombination. The solid lines represent actual transfer events. The dashed lines show other possible paths. (B) Energy level diagram. The diagram shows only one of the n acceptors.

where R is the donor–acceptor (center to center) separation. R_0 and R_b are used to parameterize the distance scales of the forward and back transfers. a_f and a_b characterize the falloff of the electronic wave function overlap between the neutral donor and acceptor levels and between anion and cation, respectively.[12,22,37] τ is the fluorescence lifetime of the donor.

The differential equations governing the process for a fixed set of acceptor distances given by R_i are

$$\frac{dP_{ex}(t)}{dt} = -(k + \sum_{i=1}^{n} K_f(R_i))P_{ex}(t) \tag{2}$$

$$\frac{dP^i_{ct}(t)}{dt} = K_f(R_i)P_{ex}(t) - K_b(R_i)P^i_{ct}(t) \qquad i = 1, ..., n \tag{3}$$

$P_{ex}(t)$ is the probability of finding the donor in its excited state. $\sum_{i=1}^{n} P^i_{ct}(t)$ describes the total probability of finding the donor in its cation state, and $P^i_{ct}(t)$ is the probability of finding the donor in its cation state with the ith acceptor in its anion state.

In the forward-transfer process the donor molecule can transfer an electron to any acceptor with the transfer rate determined by the D–A separation. The back transfer is different. The anion can transfer an electron only to the originally excited donor molecule (now a cation). Transfer from the anion to a neutral acceptor is not included since there is no net driving force for the transfer and barriers for electron tunneling are generally large.[2] Transfer from an anion to a cation which was not the original source of the electron is not included because the concentration of donors is low and the concentration of donor cations is even lower. For back transfer the distribution of cation–anion separations is not random but is dependent on the details of the forward transfer. Equation 3 properly accounts for this time-dependent distribution. The solution of eq 2 and the ensemble average of $P_{ex}(t)$ in the thermodynamic limit is straightforward and has been derived by IH.[37] The result is

$$\langle P_{ex}(t)\rangle = e^{-t/\tau}\exp[-(C/C_0)\gamma^{-3}g(e^{\gamma}t/\tau)] \tag{4}$$

Where C is the acceptor concentration and C_0 is given by $C_0 = 3/(4\pi R_0^3)$; γ is R_0/a_f with

$$g(Z) = 3\int_0^{\infty}(1 - \exp(-Ze^{-y}))y^2\,dy \tag{5}$$

Instead of directly solving eq 3 for $P^i_{ct}(t)$, and then performing the ensemble average over $P^i_{ct}(t)$ and passing to the thermodynamic limit, we first perform the ensemble average over all possible spatial configurations of $n-1$ acceptors in a volume V for each term of eq 3.

$$\left\langle \frac{dP^i_{ct}(R_i,t)}{dt}\right\rangle_{n-1} = \langle K_f(R_i)P_{ex}(R_i,t)\rangle_{n-1} - \langle K_b(R_i)P^i_{ct}(R_i,t)\rangle_{n-1} \tag{6}$$

where $\langle\ \rangle_{n-1}$ denotes an average over all spatial coordinates except the ith spatial coordinate. $\langle P^i_{ct}(t)\rangle_{n-1}$ is the averaged probability of finding the donor in its cation state with acceptor at R_i in its anion state. Since the spatial distribution of acceptors at different points is uncorrelated and the ensemble averaging procedure is

(36) Dorfman, R. C.; Lin, Y.; Fayer, M. D. *J. Chem. Phys.*, in press.
(37) Inokuti, M.; Hirayama, F. *J. Chem. Phys.* **1965**, *43*, 1978.
(38) Newell, V. J.; Rose, T. S.; Fayer, M. D. *Phys. Rev. B* **1985**, *32*, 8035.
(39) Lutz, D. R.; Nelson, K. A.; Gochanour, C. R.; Fayer, M. D. *Chem. Phys.* **1981**, *58*, 325.
(40) Lin, Y.; Dorfman, R. C.; Fayer, M. D. *J. Chem. Phys.*, in press.
(41) Dexter, D. L. *J. Chem. Phys.* **1953**, *21*, 836.

independent of the time derivative, eq 6 can be written as

$$\frac{d}{dt}\langle P^i_{ct}(R_i,t)\rangle_{n-1} = K_f(R_i)\langle P_{ex}(R_i,t)\rangle_{n-1} - K_b(R_i)\langle P^i_{ct}(R_i,t)\rangle_{n-1} \quad (7)$$

Casting the problem in the form of eq 7 has an important advantage. It reduces the many particle problem in eq 3 to a two particle problem. This is the key step which makes the solution of this problem tractable.

The solution of differential eq 7 is

$$\langle P^i_{ct}(R_i,t)\rangle_{n-1} = \int_0^t K_f(R_i)e^{-K_b(R_i)(t-t')}\langle P_{ex}(R_i,t')\rangle_{n-1}\,dt' \quad (8)$$

Equation 8 is an exact expression for the probability of a donor molecule being a cation with an anion at position R_i. $\langle P_{ct}(t)\rangle$ is obtained by averaging over the final position coordinate, summing over all N acceptors, and then taking the thermodynamic limit. The result is

$$\langle P_{ct}(t)\rangle = 4\pi C\int_0^\infty K_f(R_i)e^{-K_b(R_i)t}\int_0^t e^{-(K_f(R_i)-K_b(R_i))t'}e^{-t'/\tau}\times \exp\left(-\left(\frac{C}{\gamma^3 C_0}\right)g\left(e^{\gamma}\frac{t'}{\tau}\right)\right)dt'\,R_i^2\,dR_i \quad (9)$$

The results given in eq 4 and 9 are for point particles in an infinite continuum. However, in real systems, molecules occupy finite volumes. Therefore, some of the spatial configurations that arise in the ensemble averages for point particles should be excluded. Two acceptor molecules, or acceptor and donor molecules, cannot have overlapping volumes. At low concentrations, the number of configurations that are overcounted is negligible and no correction for excluded volume is necessary to give an accurate result. At concentrations encountered in experiment, however, excluded-volume effects can be important.

The incorporation of donor–acceptor and acceptor–acceptor excluded volume into the model has been described previously.[40] The results for the state probabilities are

$$\langle P_{ex}(t)\rangle = \exp(-kt)\exp\left(-4\pi d^{-3}\sum_{k=1}^{\infty}\frac{p^k}{k}\int_{R_m}^{\infty}(1-e^{-tK_f(R_j)})^k R_j^2\,dR_j\right) \quad (10)$$

$$\langle P_{ct}(t)\rangle = 4\pi C\int_{R_m}^{\infty}\int_0^t K_f(R_i)e^{-K_b(R_i)(t-t')}e^{-K_f(R_i)t'}e^{-t'/\tau}\times \exp\left(-4\pi d^{-3}\sum_{k=1}^{\infty}\frac{p^k}{k}\int_{R_m}^{\infty}(1-e^{-t'K_f(R_j)})^k R_j^2\,dR_j\right)R_i^2\,dR_i\,dt' \quad (11)$$

where R_m is the sum of the donor and acceptor radii, d is the diameter of the acceptor excluded volume, and $p = Cd^3$. Keeping only the first term in k of eq 10 and 11 gives eq 4 and 9. In the limit of low concentration or small donor and acceptor size, the higher order terms become insignificant and eq 10 and 11 reduce to eq 4 and 9, the point-particle results. The inclusion of donor–acceptor excluded volume in the calculation of the cation probability is obtained by using a cutoff, R_m, in the lower limit of integration in eq 10 and 11.

The concentration at which excluded volume can no longer be ignored depends not only on the excluded volumes but also on the system's electron-transfer parameters. R_m, which accounts for donor–acceptor excluded volume, is effectively a rate cutoff. R_0 and R_b are the distances at which the forward- and back-transfer rates, respectively, are equal to the rate of fluorescence, $1/\tau$. At distances shorter than R_0 and R_b the rates of forward and back transfer are faster than $1/\tau$. If R_m is very small compared to R_0 and R_b, then the effect of donor–acceptor excluded volume is negligible. If R_m is some significant fraction of R_0 and R_b, and if the concentration is sufficiently high to give a reasonable probability of finding an acceptor in a volume with radius R_m, then the averages will be different from the point-particle case. The cutoff will exclude many of the fast transfer contributors from the averages.

The acceptor–acceptor excluded volume cannot be included by a simple cutoff. The correction for acceptor–acceptor excluded volume eliminates the configurations from the calculations in which two or more acceptors have overlapping volumes.

III. Experimental Procedures

A. Sample Preparation. The samples are composed of rubrene (donor) and duroquinone (acceptor) in sucrose octaacetate glass. In the presence of light and oxygen, rubrene [RU] in solution will irreversibly oxidize. The presence of dust particles in samples increases the amount of scattered light and noise for the types of experiments addressed in this paper. Concentration inhomogeneities in the samples will lead to inconsistent results. These three problems shaped the sample preparation technique. The following is a detailed account of the preparation method.

First the glass, sucrose octaacetate [SOA], was twice recrystallized in ethanol. The electron acceptor, duroquinone [DQ], was twice sublimated. RU, the electron donor, is difficult to sublimate or recrystallize. Instead, a small amount of RU was dissolved in a degassed (with argon) solution of SOA in acetone (spectral grade) in the dark. This solution was immediately filtered through a 0.45-μm filter into a 1-mm (path length) optical cell with a long stem ($\approx$15-cm^3 volume) and ball joint glass blown onto it. The cell was placed on a vacuum line with a liquid nitrogen trap and backfilled with nitrogen to remove oxygen in the atmosphere above the solution. The pressure in the cell was gradually lowered so that the acetone could evaporate. When no more acetone could be detected by eye, the sample was melted (still under vacuum $\approx 10^{-6}$ Torr), by using a heat gun, to remove any residual acetone. The cell was removed from the vacuum line and DQ was placed in the cell. The sample was placed back on the vacuum line and sealed off. The sample was melted to help dissolve the DQ. While molten, the sample was shaken. This last step is repeated several times to ensure a homogeneous distribution of the DQ.

By preparing the samples in the dark and using degassed solutions under vacuum, RU's sensitivity to oxygen has been eliminated. Samples of RU in SOA as old as 1 year show no signs of decomposition in either their spectra or their appearance. Scattered light from dust particles has been reduced by the filtration. The problem of sample inhomogeneities has been eliminated. Inhomogeneities can be measured by taking the optical density as a function of sample position. Samples of RU in SOA prepared with the above technique show no variation in the concentration of RU. Inhomogeneities in the DQ concentration were eliminated by melting and shaking the SOA–RU–DQ solutions several times.

The concentrations of DQ and RU were determined spectroscopically. The extinction coefficient of DQ in SOA at 430 nm was measured from samples of known concentration. The result is 28.8 L/(mol·cm). The ratio of the RU in SOA extinction coefficient at 528 nm to the extinction coefficient at 430 nm is $\eta_{528}/\eta_{430} = 5.27$. This result was obtained from the ratio of the optical densities [OD]. The extinction coefficient of RU in SOA at 528 nm is 11 600 L/(mol·cm). DQ does not absorb at 528 nm. RU absorbs at 528 and 430 nm. To get the DQ optical density, it was necessary to subtract the RU contribution to the OD at 430 nm.

For the various samples, the RU OD ranged from 0.05 to 0.1, which corresponds to a concentration range of 0.5×10^{-4} to 1.0×10^{-4} M. The concentration range for DQ was 0.0–0.4 M. The low concentration of RU ensured there was no donor–donor electronic energy transfer. The donor and acceptor pair was chosen very carefully to avoid electronic excitation transport from the donor to the acceptors. This implies that the emission of the donor (RU) must not overlap with the absorption spectrum of the acceptor (DQ). Even a very small amount of spectral overlap can significantly influence the excited-state dynamics because of Forster-type excitation transfer.[42] Since the rate of excitation transfer falls off with distance much slower than the rate of

(42) Förster, Th. *Discuss. Faraday Soc.* **1959**, *27*, 7.

electron transfer ($1/R^6$ vs e^{-R}), even a small excitation transport R_0 can lead to significant contamination of the electron-transfer measurements.

B. Fluorescence Yield Measurements. The reduction in the RU quantum yield as a function of acceptor concentration was measured in the following manner. Single pulses at 0.5-kHz repetition rate from a CW pumped acoustooptically mode-locked and Q-switched Nd:YAG laser are doubled to 532 nm. The green single pulses (fwhm = 100 ps) are used for sample excitation. A sample holder was constructed to ensure that each sample was reproducibly illuminated with the same amount of light and the same solid angle of fluorescence collected. The fluorescence was collected by a lens that imaged on the slit (0.5 mm) of a 1/4-m monochromator. This was used to filter out the green excitation pulse. The detection wavelength was near the fluorescence maximum of RU at 560 nm. Detection employed a photomultiplier tube and a lock-in amplifier.

To avoid problems of laser power drift, the yield for RU in SOA (η_0) was measured immediately after measurement of each electron-transfer sample yield (η_c). Care was taken to avoid stimulated emission. To find an appropriate laser power, the relative yield (η_c/η_0) for a sample was measured as a function of laser power. At sufficiently low powers, the yield became power independent.

C. Time-Resolved Fluorescence Measurements. Rubrene's fluorescence decays were measured in samples with various acceptor concentrations in the following manner. The single green pulses (532 nm) described above were used for time-resolved fluorescence quenching measurements. The fluorescence was detected at an angle of 90° from the excitation beam through a small pinhole (1 mm) placed on the sample. This pinhole reduced reabsorption artifacts in the data. The fluorescence was collected by a lens and imaged on the slit (0.5 mm) of a double $^1/_4$-m monochromator set to pass 560 nm, the fluorescence maximum of RU. Time resolution was provided by a microchannel plate coupled to a boxcar averager. The sampling window (200 ps) of the boxcar was positioned in time by a 10-V ramp, giving a time range of 100 ns. The digital output of the boxcar was added to the data from previous shots by computer until an adequate signal to noise ratio was obtained. The overall time response of the system ($\approx$1.2 ns) was measured by observing the excitation pulse (100 ps). The system impulse response was recorded and used for convolution with theoretical calculations to permit accurate comparison to the data.

D. Transient Grating Experiments. The transient grating experiment has been described previously.[43,44] Here specific details and considerations necessary to make the electron-transfer measurements will be discussed. Two time-coincident pulses are crossed inside the sample. These coherent pulses interfere to produce an optical fringe pattern. Optical absorption by the donor molecules results in a spatial distribution of excited states that mimics the fringe pattern. Subsequent electron transfer will result in a pattern of ion pairs that also mimics the fringe pattern. The fringe pattern of the excited states and ion pairs results in a spatially periodic variation in the sample's complex index of refraction, which acts as a Bragg diffraction grating. A third picosecond pulse is brought into the sample with a variable delay time and is Bragg diffracted from the grating. The time dependence of the diffracted signal is the grating observable. The formation and recombination of the ion pairs determine the time dependence of the grating signal.

The two excitation pulses were at wavelength 532 nm (fwhm = 100 ps). The angle between the excitation beams was set to give a grating fringe spacing of 3 μm. The spot size of the probe beam was $\approx$50 μm (radius of E field) and the spot sizes of the excitation beams were each $\approx$70 μm. The probe pulse used in some experiments was also at 532 nm. The probe was brought in slightly off the Bragg angle, i.e., not quite colinear with one of the excitation beams. This results in a Bragg-diffracted signal spatially separated from the other excitation beam. It was split from the same doubled Nd:YAG pulse as the excitation beams. Alternately, a tunable dye laser was used for the probe to test for ion absorptions (see section E). The pulses from the dye laser were at 550 nm (fwhm = 30 ps) and were brought in at the Bragg angle.

In most of the experiments, the excitation beams had opposite polarizations and the probe's polarization was parallel to one of the excitation beams; this is called a polarization grating.[45] The resulting signal beam had a polarization opposite the probe's. Thus, not only was the signal spatially segregated from the other beams, but it also had a polarization opposite to that of the nearest excitation beam. The advantage of the polarization grating lies in its ability to avoid scattered light at polarizations other than the signal's. The probe beam was chopped at 250 Hz. The laser repetition rate was 500 Hz. The signal was passed through a polarizer and a monochromator set to the probe's wavelength and was detected by a photomultiplier tube. The signal was processed by a lock-in amplifier and digitized and stored in a computer. Since the probe beam was chopped, excitation beam scattered light was subtracted out by the lock-in amplifier. Probe scattered light had polarization opposite that of the signal and is eliminated by the detection polarizer.

Fluorescence from the donor can greatly increase the unwanted background. Passing the signal through a monochromator before detection filters out the fluorescence background. The monochromator enabled us to decrease pulse intensities (decreased detection lock-in scales by 3 orders of magnitude) so that we could avoid artifacts due to high power. It is important, however, to align the signal through the monochromator such that the throughput is not changed as the delay line is run over the 15 ns (15 ft) of travel.

E. Tests for Excited-State and Ion Absorptions. The extent of excited-state–excited-state (ES–ES) absorption was determined by measuring the absorption as a function of laser power in a sample of RU in SOA (corrected for scattered light by subtracting the attenuation measured in an SOA sample prepared by using the same method). At low powers the OD should be constant with power and should reflect the ground-state absorption coefficient. As power increases, the excited-state population increases. This will increase the probability for ES–ES absorption. If ES–ES absorption is small or not present, then as power increases the absorption will saturate and the apparent OD will go down at powers greater than the saturation power. Comparison of the apparent OD to the calculated saturation characteristics, including the possibility of ES–ES absorption, yields a measurement of the ES–ES absorption within experimental error. The results demonstrated that, at the probe wavelengths, neutral RU absorption occurs only from the ground state.

To test for ion absorptions at the probe wavelengths, it is necessary to compare transient grating results at two wavelengths. If the probe wavelengths fall within the absorption spectra of ions, different time-dependent curves will be obtained (see section IV) at different wavelengths. As discussed in section V, the time-dependent grating decay curves are independent of wavelength. Therefore, ion absorption is negligible.

IV. Data Analysis

The dynamics of electron transfer and back transfer are determined by five molecular parameters and the concentration of the acceptors in the sample. In addition to the donor excited-state lifetime, τ, there are four parameters, a_f and R_0 (forward-transfer parameters), and a_b and R_b (backward-transfer parameters). The forward-transfer parameters are determined by a combination of concentration-dependent fluorescence yield measurements and time-resolved fluorescence decay experiments. With knowledge of these parameters, the back parameters are obtained by using the transient grating technique, a ground state recovery experiment.

(43) Fayer, M. D. *Annu. Rev. Phys. Chem.* **1982**, *33*, 63.
(44) Dorfman, R. C.; Lin, Y.; Zimmt, M. B.; Baumann, J.; Domingue, R. P.; Fayer, M. D. *J. Phys. Chem.* **1988**, *92*, 4258.
(45) Eyring, G.; Fayer, M. D. *J. Chem. Phys.* **1984**, *81*, 4314.

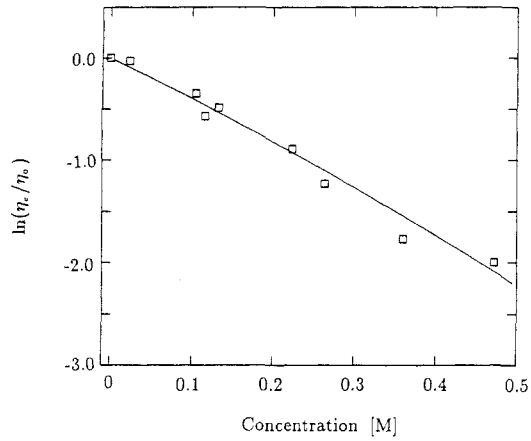

Figure 2. Relative fluorescence yield plotted as a function of the acceptor concentration. From this plot one of the two forward-transfer parameters is determined, i.e., R_0 = 13.1 Å.

Figure 2 displays the relative fluorescence yield data and the best fit to the data. From the theory,[22,37,40] an expression for the relative fluorescence yield, η_c/η_0, as a function of acceptor concentration, has been derived. Starting from eq 10, the probability that the donor is in its excited state, and integrating it over time, gives the relative fluorescence yield.

$$\eta_c/\eta_0 = \frac{1}{\tau}\int_0^\infty \langle P_{ex}(t)\rangle \, dt \tag{12}$$

In principle eq 12 depends on two forward electron-transfer parameters a_f and R_0, as well as concentration C. However, Inokuti and Hirayama[37] have found that η_c/η_0 is not sensitive to large changes of the a_f value for the case without excluded volume. Our numerical tests show that their result is true even when excluded-volume effects are considered. Therefore, by comparing steady-state fluorescence yield data to the η_c/η_0 obtained from eq 12, we are able to uniquely determine the forward-transfer parameter R_0. For RU (donor) and DQ (acceptor) in SOA glass at room temperature, R_0 is 13.1 Å. It is in effect a single parameter fit.

The time-resolved fluorescence quenching data are presented in Figure 3. $\langle P_{ex}(t)\rangle$ was calculated and convolved with the instrument response function, $F(t)$.

$$I(t) = \int_{-\infty}^{t} F(t') \, \langle P_{ex}(t-t')\rangle \, dt' \tag{13}$$

Equation 13 was fit to the data using one adjustable parameter a_f and R_0 = 13.1 Å. The rubrene lifetime, τ = 16.5 ns, employed in the calculations was measured with the transient grating experiment. As can be seen in Figure 3, there is a unique fit for all concentrations, although the fits undershoot the data slightly at long times. The undershoot is a consequence of a very small amount of fluorescence reabsorption which appears to make the lifetime measured by fluorescence slightly longer than the actual τ. The transient grating experiment is much less sensitive to reabsorption effects because the distance scale is the fringe spacing (a few microns) rather than the laser spot size (a few hundred microns). The small deviation at long time does not influence the value of a_f. The best fit yields a_f = 0.22 Å.

The transient grating signal, $S(t)$, is proportional to the square of the peak–null difference in the complex index of refraction of the medium.[46-48] The excitation and probe wavelengths do not excite the acceptor (A) but are chosen to be within the strong ground-state to first excited-state absorption of the donor (D). Reduction in the number of ground-state donors upon excitation

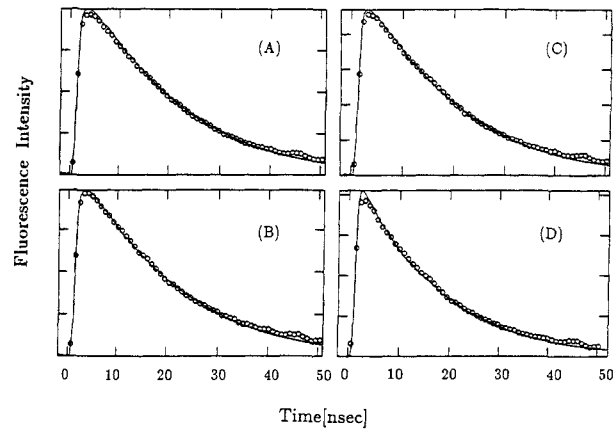

Figure 3. Time-resolved fluorescence data and theory shown for four concentrations. The circles are the experimental data, and the lines are the theoretical curves. Plot A has an acceptor concentration of 0.105 M, plot B is 0.134 M, plot C is 0.224 M, and plot D is 0.470. Only a_f was adjusted to fit these curves, giving a_f = 0.22 Å.

causes a change in the index of refraction at the grating peaks. It is also possible, however, for the probe wavelength to fall on an excited-state donor absorption (D^*), a cation adsorption (D^+), or an anion absorption (A^-). Any of these absorptions will also contribute to the change in the peak–null index of refraction because they have the same spatial periodicity in concentration as the ground-state depleted donors. The real and imaginary parts of the peak–null difference in the index are given by eq 14 and 15, respectively

$$\Delta n = \Delta n_D + \Delta n_{D^*} + \Delta n_{D^+} + \Delta n_{A^-} \tag{14}$$

$$\Delta k = \Delta k_D + \Delta k_{D^*} + \Delta k_{D^+} + \Delta k_{A^-} \tag{15}$$

where Δn_D is the difference in the real part of the index between the grating peaks and nulls for the donor's ground state. Similarly, Δn_{D^*}, Δn_{D^+}, and Δn_{A^-} are the possible contributions to the peak–null differences from the donor's excited state, the donor's cation state, and the acceptor's anion state. The Δk's are the peak–null differences in the imaginary part of the index.

The grating signal is related to the sum of the squares of eq 14 and 15

$$S(t) = B_1(\Delta n)^2 + B_2(\Delta k)^2 \tag{16}$$

where B_1 and B_2 are time-independent constants that involve the wave vector matching condition, the probe intensity, beam geometries, etc. (It is important to recognize that, in a transient grating experiment, the solvent can contribute to the signal through the Kerr effect[45,49,50] even if the solvent does not absorb at the excitation wavelength. It is necessary to check a solvent blank to assure that the solvent does not contribute to the signal. SOA did not give a signal in the absence of Ru.)

The terms in eq 14 and 15 are proportional to quantities calculated by theory.[40]

$$\Delta n_D \text{ and } \Delta k_D \propto (\langle P_{ex}(t)\rangle + \langle P_{ct}(t)\rangle) \tag{17}$$

$$\Delta n_{D^*} \text{ and } \Delta k_{D^*} \propto \langle P_{ex}(t)\rangle \tag{18}$$

$$\Delta n_{D^+} \text{ and } \Delta n_{A^-} \text{ and } \Delta k_{D^+} \text{ and } \Delta k_{A^-} \propto \langle P_{ct}(t)\rangle \tag{19}$$

For the RU–DQ in SOA system eq 16 can be simplified. The saturation study, described in the Experimental Section, on RU in SOA showed there was no detectable ES–ES absorption. Thus Δn_{D^*} and Δk_{D^*} are zero.

The relative contributions of the other terms to the signal depend on the probe's wavelength, since the various species will not have the same absorption spectra. Thus the contributions from the various terms will change with wavelength, and the observed time

(46) Nelson, K.; Casalegno, R.; Miller, R. J. D.; Fayer, M. D. *J. Chem. Phys.* **1982**, *77*, 1144.
(47) Collier, R.; Burckhardt, C. B.; Lin, L. H. *Optical Holography*; Academic: New York, 1971.
(48) (a) Kogelnik, H. *Bell Syst. Tech. J.* **1969**, *48*, 2909. (b) Kubota, T. *Opt. Acta* **1978**, *25*, 1035.
(49) Deeg, F.; Fayer, M. D. To be published.
(50) Ruhman, S.; Williams, L. R.; Joly, A. G.; Nelson, K. A. *IEEE J. Quantum Electron.* **1988**, *24*, 470.

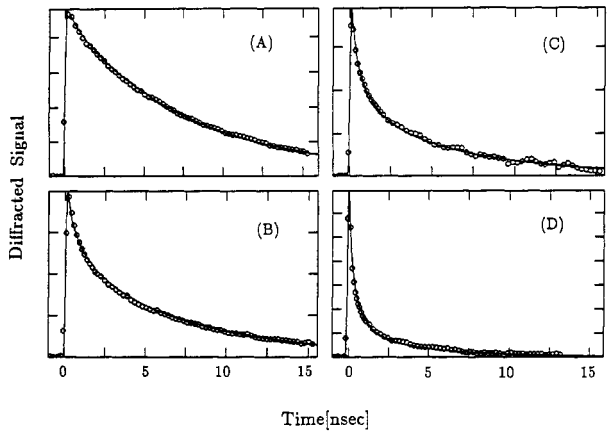

Figure 4. Transient grating data and theoretical fits given for four different concentrations. The circles are the experimental data, and the lines are the theory. Plot A is 0.024 M, plot B is 0.134 M, plot C is 0.224, and plot D is 0.470 M in acceptor concentration. All curves were fit with one set of parameters; R_b = 13.5 Å and a_b = 0.8 Å.

dependence will also change. The probe wavelengths fall within the D absorption. If the probe wavelength is changed within the known D absorption band, and the time-dependent signal does not change, then only Δn_D and Δk_D are contributing to the signal. As discussed above, the time dependence of the signal in these experiments is independent of the probe wavelength. Therefore

$$S(t) = B_1(\Delta n_D)^2 + B_2(\Delta k_D)^2 \quad (20)$$

These two terms have the same time dependence. (If in a particular experimental donor–acceptor system, the signal is dependent on the probe wavelength, time-dependent data taken at two or more wavelengths combined with the theoretical expressions for the various probabilities will permit complete analysis of the experiments.)

Using eq 20, in terms of the state probabilities, the signal is

$$S(t) = S_0[\langle P_{ex}(t)\rangle + \langle P_{ct}(t)\rangle]^2 \quad (21)$$

The time-independent constant, S_0, which determines the size of the signal, depends on factors such as the donor extinction coefficient, the laser pulse energy, the spot size, the beam crossling angle, sample thickness, and donor concentration.[43,45] $\langle P_{ex}(t)\rangle$ is the donor excitation survival probability, given in eq 10, and $\langle P_{ct}(t)\rangle$ is the cation state probability from eq 11.

Figure 4 presents transient grating data for several concentrations of acceptors with fits through them. The theoretical curves presented in the figure were convolved with Gaussian-shaped excitation pulses and probe pulse in the appropriate manner given by

$$I(t) = \int_{-\infty}^{\infty} R_p(t')\left[\int_{-\infty}^{t-t'} R_e(t'')S(t-t'-t'')\,dt''\right]^2 dt' \quad (22)$$

where $R_p(t)$ and $R_e(t)$ are the pulse-shape functions for the probe and excitation beams, respectively. $S(t)$ is the transient grating signal for δ-function pulses, calculated from eq 21. The convolution is essential since the decays are highly nonexponential. The pulse durations and shapes were determined using a transient Kerr grating in CS_2 liquid. Since the CS_2 rotation time (1.6 ps) is very fast compared to the pulse durations, the instrument response can be obtained and the pulse shapes can be determined.

In the calculations, the excluded-volume theory was employed. The sum of the donor and acceptor radii, R_m, used in the calculations is 9.0 Å. The diameter, d, of the acceptor excluded volume is 7.2 Å. These numbers were obtained from the densities of pure RU and pure DQ crystals at room temperature. In the initial report of the theory, excluded-volume effects were not included and data was fit by using the point-particle model.[44] The fits with excluded-volume effects give the correct parameters which are significantly different from those reported previously. Separate calculations showed that both donor–acceptor and acceptor–acceptor volume effects are important. Numerical illustrations of these effects are given in ref 40. Although using the excluded-volume theory is important to obtain accurate electron-transfer parameters, there is some leeway in the exact sizes used for R_m and d. Calculations showed that the same electron-transfer parameters were obtained for changes in R_m and d of greater than 10%. This should also imply that a spherical model of the molecular volume, as is used here, is adequate.

The parameters determined by the fits to the transient grating data are R_b = 13.5 Å and a_b = 0.8 Å. Although the transient grating data analysis required two parameters there was a strong minimum in χ^2 for the calculated curves going through the data at the various concentrations. This ensured a unique fit. The excellent agreement between theory and experiment displayed in Figure 4 demonstrates that the theoretical expressions provide a detailed description of the dynamics of electron transfer and back transfer for randomly distributed donors and acceptors in solid solution.

The close agreement between theory and experiment demonstrates that the distance dependence used in the electron-transfer model is sufficient to describe the transfer dynamics. In the model the transfer rates were independent of angles and local solvent structure. A previous study[12] has shown that, in principle, the time-resolved fluorescence observables are dependent on the form of the angular dependence of the electron-transfer rate. However, after performing the angular and spatial ensemble averages, the deviations from the IH model were shown to be negligibly small. A similar situation is expected for the effects of the distribution of solvent structures which can give rise to a distribution of energy gaps (ΔG).[51] In the room temperature glass system employed in the experiments presented here, thermal fluctuations are likely to wash out the effects of a distribution of energy gaps on the electron-transfer rate. For situations where temperature fluctuations are much smaller than the distribution of energy gaps, Mataga et al.[51] have derived a theory that accounts for the distribution. However, as with the angular average, the ensemble average over ΔG's is unlikely to generate decays that differ significantly from the IH form.

V. Results and Discussion

In the previous section four electron-transfer parameters were obtained from fluorescence yield, time-resolved fluorescence quenching, and transient grating experiments. A comparison of the measured forward and back parameters shows that the forward electron transfer has a shorter distance scale and attenuates more quickly than the back transfer. This trend[6,9] has been observed in other systems. Beratan[6] has shown that in porphyrin–linker–quinone systems, where the donor (porphyrin) is held at a fixed distance from the acceptor (quinone) by a rigid molecular bridge, the ratio of the forward attenuation constant to the back (a_f/a_b) is ≈0.56.[52]

It has been shown[7,9,18,19,27] that electron-transfer rates as a function of $\Delta G°$ initially increase (normal region), reach a maximum, and then decrease (inverted region) with increasing exothermicity. An explanation for the different forward and back rates has been suggested in terms of the exothermicities of the forward and back rates. Brunschwig et al.[9] suggests that the forward electron transfer might be in the normal region while the back transfer is in the inverted region. Although both the normal and inverted regions have been observed for charge recombination, only the normal region has been observed for charge separation.[53,54]

The value for a_b = 0.8 Å is more typical than the value a_f = 0.22 Å. Other values for the attenuation constant are 0.7 Å (tris[3,4,7,8-tetramethylphenanthroline]ruthenium(II) (cation donor) and methylviologen (cation acceptor) in glycerol at 250 K),[22] and 0.83 Å (biphenyl radical anions and neutral organic acceptors in 2-methyltetrahydrofuran at 77 K).[27]

(51) Toshiaki, K.; Mataga, N. *J. Phys. Chem.* **1988**, *92*, 5059.
(52) Note Beratan gives α^{for} = 0.9 Å^{-1} and α^{rev} = 0.51 Å^{-1}, where $a = 1/\alpha$.
(53) Mataga, N.; Kanda, Y.; Asahi, T.; Miyasaka, H.; Okada, T.; Kakitani, T. *Chem. Phys.* **1988**, *127*, 239.
(54) Mataga, N.; Kanda, Y.; Asahi, T.; Miyasaka, H.; Okada, T.; Kakitani, T. *Chem. Phys.* **1988**, *127*, 249.

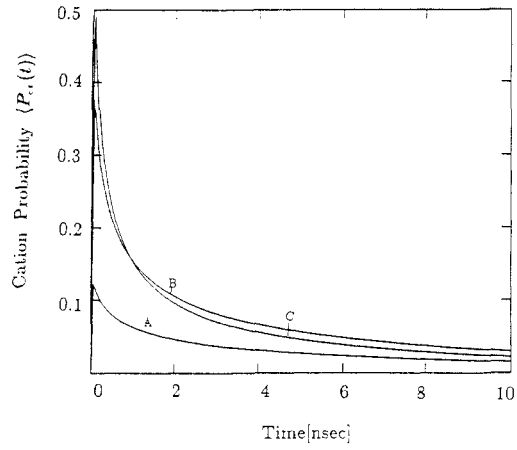

Figure 5. Ensemble-averaged rubrene cation probability for three duroquinone acceptor concentrations. Curve A is 0.064 M, curve B is 0.264 M, and curve C is 0.470 M in acceptor concentration. The electron-transfer parameters used in the calculations are obtained from the experiments.

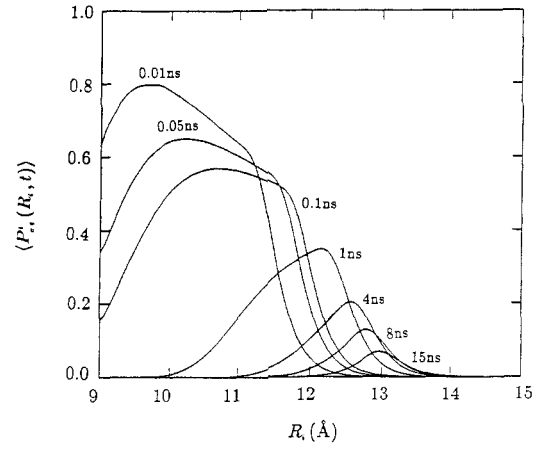

Figure 6. Probability that the ith acceptor is an anion as a function of distance at particular times. At short times the anions are found close to the cations. At longer times the anion–cation separation moves out. The acceptor concentration $C = 0.264$ M. The electron-transfer parameters used in the calculations are obtained from the experiments.

With the forward and back parameters we are able to calculate a number of interesting time- and distance-dependent properties characteristic of electron transfer and recombination. Numerical results for the ensemble-averaged cation probabilities, $\langle P_{ct}(R,t)\rangle$, the average cation–anion separation distance $\langle R(t)\rangle$, and average cation existence time $\langle \tau(R)\rangle$ will be discussed.[40]

A. The Cation Probabilities. Figure 5 shows calculations of the ensemble-averaged time evolution of the cation probability $\langle P_{ct}(t)\rangle$, eq 11, for various acceptor concentrations. The electron-transfer parameters R_0, R_b, a_f, and a_b and the lifetime, τ, are obtained from the experiments. One observes that $\langle P_{ct}(t)\rangle$ rises rapidly within the first 100 ps, reaches its maximum value, and then slowly decays to zero. At $t = 0$, the donor molecules are in their excited states, and no ion pairs exist; hence $\langle P_{ct}(t)\rangle = 0$. After excitation, a fraction of the systems in the ensemble will fluoresce and a fraction will undergo forward electron transfer. As a result of electron transfer, the cation-state population builds up. The onset of radical pair formation marks the beginning of the recombination process. The competition between the probabilities of forward electron transfer and recombination determines the detailed shape of $\langle P_{ct}(t)\rangle$. Figure 5 shows that the maximum cation probability increases as the acceptor concentration increases, that is going from curves A to B to C. After their maxima, the higher concentration curves decay more rapidly. Increasing the concentration of the acceptor molecules greatly increases the short-range electron-transfer events. In the next subsection it will be shown that increasing the acceptor concentration reduces the average cation existence time.

For a system of randomly distributed donors and acceptors, it is possible to look at the influence of a particular acceptor on the cation probability as a function of time and donor–acceptor separation. To investigate the effect of the ith acceptor, it is necessary to average over the positions of all other acceptors, since they in part determine the rate of electron transfer to the ith acceptor when it is at location R_i. The expression for this conditional probability[40] is

$$\langle P^i_{ct}(R_i,t)\rangle = \begin{cases} 0 & \text{if } R_i < R_m \\ \int_0^t K_f(R_i) e^{-K_b(R_i)(t-t')} \langle P_{ex}(t')\rangle \, dt' & \text{otherwise} \end{cases} \tag{23}$$

It is informative to plot cross sections of this two-dimensional surface as functions of time at constant distance and distance at constant time. These plots are shown in Figures 6 and 7.

$\langle P_{ct}(R_i,t)\rangle$ vs distance for a unit volume element about R_i is displayed in Figure 6 for the time, t, varying from 0.01 to 15 ns. The electron-transfer parameters are those obtained from the experiments, and the concentration of the acceptors is 0.264 M. For a given time, the curves show the probability of having ion

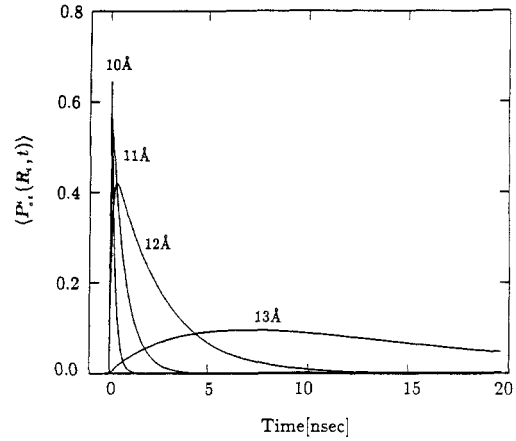

Figure 7. Probability that the ith acceptor is an anion as a function of time at particular distances. This illustrates the dramatic differences that occur with relatively small change in distance. The electron-transfer parameters used in the calculations are obtained from the experiments.

pairs with various ion separation distances. Consider one of the curves for a particular time, t. If each point on the curve is multiplied by $4\pi C R_i^2$, and integrated, the resulting value corresponds to the value of curve B in Figure 5 at that time.

In Figure 6, for each time, there is a most probable cation–anion separation, and this distance increases as t increases. At short time, most ion pairs that are created have small ion separations. These pairs are created quickly, but becuase of the small separations, recombination is very rapid. Thus, the pairs created at short time with small ion separations do not survive for very long. As time increases, the ion separation becomes larger. As can be seen from the figure, it is as if the distribution of separations moves out as a damped wave. It can also be seen from the figure that there is an effective maximum separation. This arises because the excited-state lifetime acts to cut off very slow, long-range-transfer events.

The asymmetry of $\langle P_{ct}(R_i,t)\rangle$ at short time in Figure 6 results from the difference in the electron-transfer parameters a_f and a_b. From the experiments we have $a_f = 0.22$ Å, $a_b = 0.8$ Å, $R_0 = 13.1$ Å, and $R_b = 13.5$ Å. Equations 1b and 1c indicate that this particular combination of a_f and a_b makes the forward electron-transfer rate faster than the recombination rate for $R \leq R_0$ and slower than recombination for $R \geq R_b$. Thus, at short distances the forward rate rapidly increases the ion population. At larger separations, the recombination rate dominates, and a steep falloff in the ion concentration results.

Figure 7 exhibits the dependence of $\langle P_{ct}(R_i,t)\rangle$ on time for distances R_i, varying from 10 to 13 Å. The parameters used in the calculation are again the same as those used to fit the ex-

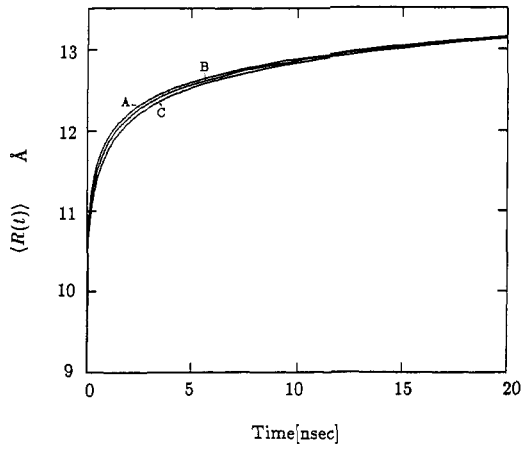

Figure 8. Average ion separation as a function of time. The ion pairs with small separations recombine rapidly and are removed from the average over distance. The result is the rapid increase in separations at short times. The parameters in the calculations are obtained from the experiments. Curve A is 0.064 M, curve B is 0.264 M, and curve C is 0.470 M in acceptor concentration.

perimental data. For a given t, if the value for a particular distance is multiplied by $4\pi CR_i^2$ and then integrated over all distances, the resulting number is the value of curve B in Figure 5 at time t. Like Figure 6, these curves give a feel for the partitioning of ion-pair separations by time intervals. For example, at 5 ns, pairs separated by 10 Å have been created and recombined. Pairs with 11-Å separations have almost disappeared. There are still a significant number of pairs with 12-Å separations, but they are rapidly vanishing, while the probability of finding pairs with 13-Å separation is just reaching a maximum.

B. Ion Separations and Existence Times. In this section, the average separation between ion pairs, $\langle R(t)\rangle$, and the average cation existence time, $\langle \tau(R)\rangle$, are calculated. For ion pairs, the average separation, $\langle R(t)\rangle$, is defined as[40]

$$\langle R(t)\rangle = \frac{4\pi \int_0^\infty \langle P_{ct}^i(R_i,t)\rangle R_i^3 \, dR_i}{4\pi \int_0^\infty \langle P_{ct}^i(R_i,t)\rangle R_i^2 \, dR_i} \qquad (24)$$

where $\langle P_{ct}(R_i,t)\rangle$, eq 23, is the ensemble-averaged probability of finding an ion pair at time t with separation R_i. The integral in the denominator is the normalization factor.

Figure 8 shows the average ion separation as a function of time for three different concentrations. The calculation parameters are the same as those used to fit the data. An abrupt change is observed in the first nanosecond of each curve. The curves then become relatively flat. Comparing Figures 5 and 8, we find that the rapid increase in the cation separation corresponds to the rapid increase in the cation probability. The ion pairs created at short times have small separations and recombine rapidly. The pairs that are created at longer times have larger separations and survive for much longer, giving rise to an increase in the average separation. Figure 8 also shows the effect of changing acceptor concentrations. Increasing acceptor concentration reduces the average cation–anion separation distance, but only slightly. This is discussed below.

In a previous publication,[40] the manner in which forward and back parameters affect the shape and magnitude of the cation probability and therefore $\langle R(t)\rangle$ was discussed. As an example, Figure 9 has two curves. Curve A is the same as curve C in Figure 8. For curve B, the back electron-transfer rate has been reduced by decreasing R_b. The figure shows that decreasing the back rate also decreases $\langle R(t)\rangle$. This occurs because the principle influence of decreasing the recombination rate is to allow more anions at short distances from cations to survive at a given time.

In Figure 10 $\langle R(t)\rangle$ is plotted for three concentrations. In Figure 10A the forward rate is greater than the recombination rate. Here $\langle R(t)\rangle$ shows a significant dependence on concentration. In Figure 10B the forward rate is less than the recombination rate and there is virtually no concentration dependence. The parameters obtained from experiment and used in Figure 8 give $K_f > K_b$ for $R < 13$ Å and $K_f < K_b$ for $R > 13$ Å. Therefore, the experimental system is a mixed situation. Looking at Figure 6, at short times only the short-distance events are playing a significant role. Thus at short times in Figure 8, $K_f > K_b$ and, like Figure 10A, there is some concentration dependence. At longer times in Figure 8 the concentration dependence disappears and the three curves coalesce. At longer times events happening at distances greater than 13 Å ($K_f < K_b$) are playing a significant role.

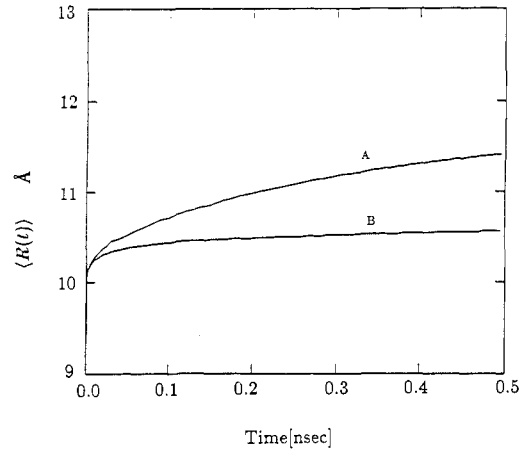

Figure 9. Average ion separation as a function of time for $C = 0.470$ M. Curve A is the same as curve C in Figure 8. Curve B uses the measured parameters except $R_b = 10.0$ Å. This reduces the back-transfer rate.

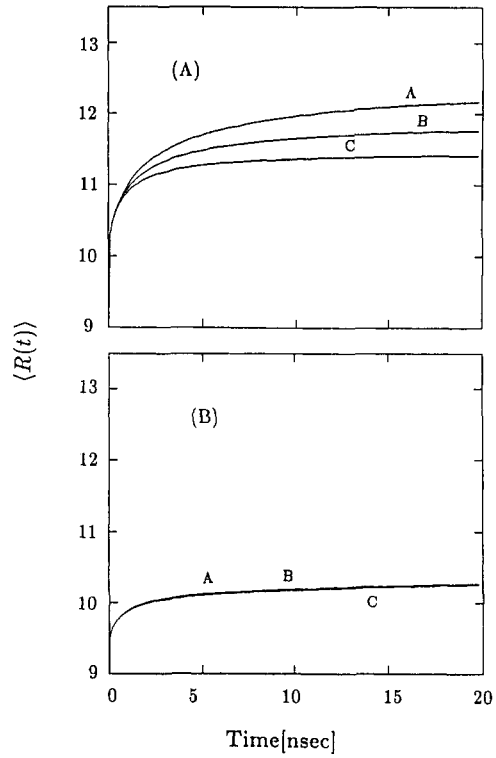

Figure 10. Average ion separation as a function of time. (A) $K_f > K_b$ and the parameters are $R_0 = 14.0$ Å, $a_f = 1.0$ Å, $R_b = 7.0$ Å, and $a_b = 0.5$ Å. (B) $K_f < K_b$ and the parameters are $R_0 = 7.0$ Å, $a_f = 0.5$ Å, $R_b = 14.0$ Å, and $a_b = 1.0$ Å. The other parameters are the same as those used in the data fits. Curve A is 0.064 M, curve B is 0.264 M, and curve C is 0.470 M in acceptor concentration.

An explanation for this seemingly nonintuitive concentration dependence lies in the fact that the forward and back electron-transfer processes are statistically different. The forward electron transfer depends on a random distribution of acceptors, any one of which could receive the electron. The greater the concentration, the greater the probability for forward transfer. The back transfer

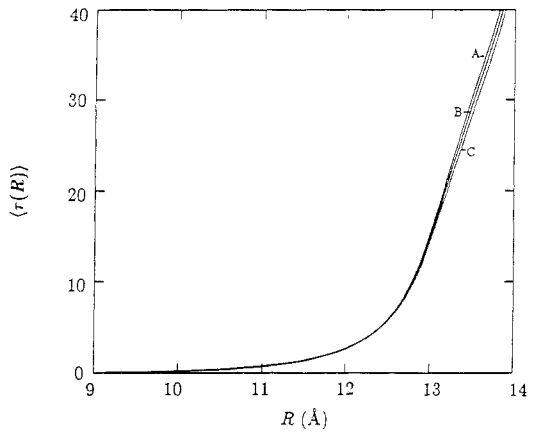

Figure 11. Average ion existence time as a function of distance. $\langle\tau(R)\rangle$ reflects the time at which ion pairs, with a particular ion separation, are likely to exist. At short distances ions will recombine rapidly while at larger distances ions will have longer existence times. The parameters are obtained from the experiments. Curve A is 0.064 M, curve B is 0.264 M, and curve C is 0.470 M in acceptor concentration.

is different. It is a single acceptor problem; the anion back transfers to the cation. It depends on the distribution of ion pairs set up by the forward electron-transfer process, which involves the concentration in a complex manner. Thus, when the forward transfer dominates ($K_f > K_b$), one should expect a greater dependence on concentration. When the recombination dominates ($K_f < K_b$), $\langle R(t)\rangle$ should be less sensitive to changes in concentration.

The average cation existence time is defined as

$$\langle\tau(R_i)\rangle = \frac{\int_0^\infty t\langle P_{ct}^i(R_i,t)\rangle\, dt}{\int_0^\infty \langle P_{ct}^i(R_i,t)\rangle\, dt} \qquad (25)$$

where $t = 0$ is the time at which the ensemble of donors is excited. It is important to note that $\langle\tau(R)\rangle$ is not the average lifetime of the ion pairs, since the ion pairs are created at various times. Therefore, for a given ion separation, the average existence time is a function of when the pairs are created and when back electron transfer returns the molecules to their neutral ground states. $\langle\tau(R)\rangle$ reflects the time at which ion pairs with a particular ion separation are likely to exist.

Figure 11 displays $\langle\tau(R)\rangle$ for several acceptor concentrations. The parameters are those obtained from the data fits. Consider curve B in Figure 11. For this concentration the ion probability as a function of time is given by curve B in Figure 5. At 12 Å, the average existence time is 3 ns. At this time the cation probability is still substantial but tailing off. At 14 Å the existence time has increased to 40 ns; however, the ion probability has decayed virtually to zero by this time. Figure 11 shows that the smallest distance scale one can probe is limited by the time resolution of the instrumentation. Consider an experiment having 10-ns time resolution. The dynamics of ion pairs having separation of 12.8 Å or greater are probed. If the time resolution is reduced to 1 ns, distances on the order of 11 Å and greater are probed. It is clear that, for the parameters of Figure 11, picosecond time resolution will be required to examine the creation and recombination of pairs with ion separations smaller than 10 Å.

VI. Concluding Remarks

We have presented the results of experimental studies of electron transfer from optically excited donors to randomly distributed acceptors followed by electron back transfer in a rigid solution. The forward electron-transfer process was observed by fluorescence yield measurements and time-dependent fluorescence quenching measurements, while the electron back transfer from the radical anion to the radical cation was monitored by using the picosecond transient grating (TG) technique. A statistical mechanics theory which describes the electron-transfer and back-transfer dynamics was employed to extract the electron-transfer parameters from the data. The theory is demonstrated to be accurate for a wide range of the concentrations.

The electron-transfer parameters obtained experimentally enabled us to construct a detailed picture of the electron-transfer process in space and time. The numerical calculations for the cation probabilities, the average cation–anion separation distance, $\langle R(t)\rangle$, and the average cation existence time, $\langle\tau(R)\rangle$, provide insights into the distance and time dependence of the flow of electron probability in an ensemble of donors and acceptors.

We have found that the transient grating technique is well suited for the study of the forward and recombination dynamics in an electron-transfer system. The grating method permits many of the problems associated with pump–probe experiments to be avoided. The experiments reported here were performed in rigid systems. The distribution of relative distances between donors and acceptors did not change with time. The theory outlined in section II is being extended to include the motions of the donors and the acceptors in liquid solutions. Thus, experiments analogous to those presented here can be conducted in liquid systems. We are also extending these studies to include the effect of solvent relaxation. Solvent relaxation will influence the very short time (less than ~10 ps) behavior of the back-transfer dynamics. Theoretical calculations of the ensemble-averaged dynamics including solvent relaxation are near completion. Subpicosecond grating experiments will be used to examine the short time behavior of the transfer back-transfer problem.

Acknowledgment. This work was supported by the Department of Energy, Office of Basic Energy Sciences (DE-FG03-84ER13251). Additional equipment support was provided by the National Science Foundation, Division of Materials Research (DMR 87-18959).

Registry No. Rubene, 517-51-1; duroquinone, 527-17-3; sucrose octaacetate, 126-14-7.